Ratcheting analysis of joined conical cylindrical shells

Jaskaran Singh[a] and B.P. Patel[*]

Department of Applied Mechanics, Indian Institute of Technology Delhi, Hauz Khas, New Delhi 110016, India

Abstract. The ratcheting and strain cyclic behaviour of joined conical-cylindrical shells under uniaxial strain controlled, uniaxial and multiaxial stress controlled cyclic loading are investigated in the paper. The elasto-plastic deformation of the structure is simulated using Chaboche non-linear kinematic hardening model in finite element package ANSYS 13.0. The stress-strain response near the joint of conical and cylindrical shell portions is discussed in detail. The effects of strain amplitude, mean stress, stress amplitude and temperature on ratcheting are investigated. Under strain symmetric cycling, the stress amplitude increases with the increase in imposed strain amplitude. Under imposed uniaxial/multiaxial stress cycling, ratcheting strain increases with the increasing mean/amplitude values of stress and temperature. The abrupt change in geometry at the joint results in local plastic deformation inducing large strain variations in the vicinity of the joint. The forcing frequency corresponding to peak axial ratcheting strain amplitude is significantly smaller than the frequency of first linear elastic axial vibration mode. The strains predicted from quasi static analysis are significantly smaller as compared to the peak strains from dynamic analysis.

Keywords: ratcheting; cyclic loading; finite element analysis; conical-cylindrical shell; quasi-static; dynamic

1. Introduction

Structural components in nuclear, chemical or power plants are often subjected to cyclic thermo-mechanical loading in their service life. Sometimes, the combination of such loads can surpass the elastic limit thereby making the structure yield. The plastic deformation may continue to accumulate cycle by cycle such that the geometry of the component gets distorted and it becomes unserviceable due to excessive deformation. This phenomenon of accumulation of plastic deformation in every cycle is known as ratcheting and the accumulated plastic strain is known as ratcheting strain. Ratcheting takes place under asymmetrical stress-controlled cycling i.e., some non-zero mean stress should exist. Ratcheting is one of the important factors in the design of components subjected to cyclic loads leading to inelastic deformation.

Various piping components of different materials have been studied experimentally to investigate cyclic behavior of structures by Benham (1965), Benallal *et al.* (1989), Hassan *et al.* (1992), Hassan and Kyriakides (1992), Delobelle *et al.* (1995), Kang *et al.* (2002), Zakavi *et al.*

---

*Corresponding author, Professor, E-mail: bppatel@am.iitd.ac.in; badripatel@hotmail.com
[a]M.Tech. Student, E-mail: jaskaransingh1989@gmail.com

(2010), Shariati *et al.* (2012), Chen *et al.* (2013). Only limited shape of geometries have been tested experimentally (Chen *et al.* 2013). Straight and elbow pipes are the most typical structural components investigated along with tee joints and lateral nozzles. The uniaxial experiments were both stress controlled and strain controlled whereas the multiaxial experiments mostly consisted of a constant primary load applied in one direction (which will lead to plastic state) and a cyclic secondary load applied in the other direction. The strain controlled experiments were mostly done for uniaxial cases to study cyclic hardening and cyclic softening characteristics or to determine material parameters for various ratcheting models available. The stress controlled experiments have been done to investigate cyclic responses like elastic shakedown, plastic shakedown and ratcheting.

The elasto-plastic response of materials can be modeled either by isotropic or kinematic hardening. Materials either cyclically harden or soften or show a combination of both when subjected to cyclic loads. Experimental studies by Hassan and Kyriakides (1994a, b) indicate that cyclic hardening and cyclic softening tend to cease after certain number of cycles and size of the yield surface stabilizes. However, ratcheting keeps on occurring with the loading cycles even after the material stabilizes. Kinematic hardening is considered to be the primary reason for ratcheting response whereas isotropic hardening mostly influences the change in the rate of ratcheting during initial cycles. Hence ratcheting aspects cannot be captured by isotropic hardening under stress controlled loading history. Therefore, kinematic hardening models are used to analyze ratcheting (Rahman 2006).

Various strain hardening models have been developed in the last three decades to predict uniaxial and multiaxial ratcheting and new modifications have also been suggested (Jiang and Kurath 1996, Corona *et al.* 1996). The first linear kinematic hardening model was proposed by Shield and Ziegler (1958). This is the simplest kinematic hardening rule to simulate plastic response of materials. This model can represent Bauschinger effect in cyclic loadings but it fails to predict ratcheting and produces a closed hysteresis loop in asymmetrical loading (Bari and Hassan 2000).

Prager's bilinear stress-strain rule was extended to multilinear form by Besseling (1959), Mroz (1967). These models are known as multilinear models. Mroz introduced the concept of a 'field of work-hardening moduli'. He suggested that in case of simple tension-compression, the stress-strain curve can be divided into a large number of linear segments with constant hardening modulus of each segment. In order to implement the model for a multiaxial generalization, a set of non-intersecting hyper surfaces are considered with separate regions of constant hardening moduli which can contract and translate together. Mroz's model can describe the cyclic hardening and softening characteristics of materials and nonlinear stress strain curve. Mroz's idea was further pursued by Dafalias and Popov (1976) by using a two surface model and defining a continuous variation of the plastic modulus between these two surfaces rather than a piecewise constant plastic moduli. These hardening rules can model plastic response of materials more accurately, but fail to predict ratcheting.

Frederick and Armstrong (1966) modified the Prager's kinematic hardening model by introducing an additional term referred to as recovery term incorporating the fading memory effect of the plastic strain path making Armstrong-Frederick (A-F) rule nonlinear in nature. The A-F model is the basic nonlinear kinematic hardening rule to predict ratcheting. It predicts constant ratcheting rate for a constant amplitude stress controlled cyclic loading and over estimates ratcheting. Thus the basic concept of A-F model has been extended by various researchers by modifying the recovery term. Chaboche (1986) decomposed the backstress into several

components where each of the components is additive in nature and obeys A-F hardening law. Further improvements were suggested by Chaboche (1991), Jiang and Sehitoglu (1994), Ohno and Wang (1993a, b), Bari and Hassan (2000) which gave more accurate simulations for ratcheting. These improvements concentrated on the non linear term of the kinematic hardening model proposed by Armstrong and Frederick.

Quite a large number of studies have been carried out in the field of ratcheting and in the formulation of its constitutive models (Dong *et al.* 2006, *Kang et al.* 2002, Kang 2008, Mahmoudi *et al*. 2011a, b, Badnava *et al*. 2012, Chen *et al*. 2013). The cone-cylinder junctions, used extensively in pressure vessels, piping, aerospace structures, fluid reservoirs, are among the simplest junctions featuring meridional slope mismatch between the connected shell elements. To the best of the authors' knowledge, the ratcheting behaviour of joined conical cylindrical shells has not been reported in the open literature. Further, most of the studies are based on quasi-static analysis without considering inertia effects. The main objective of the present work is ratcheting analysis of joined conical-cylindrical shells under non proportional uniaxial and multiaxial cyclic loading with/without the inclusion of inertia effects.

2. Chaboche's Kinematic hardening model

In this study, Chaboche's nonlinear kinematic hardening model (Chaboche 1986) is used which primarily involves superposition of three Armstrong-Frederick kinematic hardening rules (Frederick and Armstrong 1966) in the form

$$d\alpha = \frac{2}{3} C d\varepsilon^p - \gamma \alpha d\varepsilon_{eq}^p \tag{1}$$

where the recovery term (2nd term in Eq. (1)) represents the memory of the strain path history. For a uniaxial stress cycle with mean stress, the recovery term in the Armstrong-Frederick kinematic hardening rule produces changes in shapes between forward and reverse loading paths. Therefore, the loop does not close and results in ratcheting.

The kinematic hardening variable '$\boldsymbol{\alpha}$' (back stress) is composed of two parts. The first part is proportional to the plastic strain increment and the second part is the memory term. Three decomposed rules of the Chaboche model can be expressed by superimposing the backstress term as

$$d\boldsymbol{\alpha} = \sum_{k=1}^{3} d\alpha_k$$
$$d\alpha_k = \frac{2}{3} C_k d\varepsilon^p - \gamma_k \alpha_k d\varepsilon_{eq}^p \tag{2}$$

where $\boldsymbol{\alpha}$ and $\mathbf{d\varepsilon^p}$ are the backstress and the plastic strain increment tensors, respectively. C_k and γ_k are the material constants. $d\varepsilon_{eq}^p$ is the equivalent incremental plastic strain.

3. Results and discussion

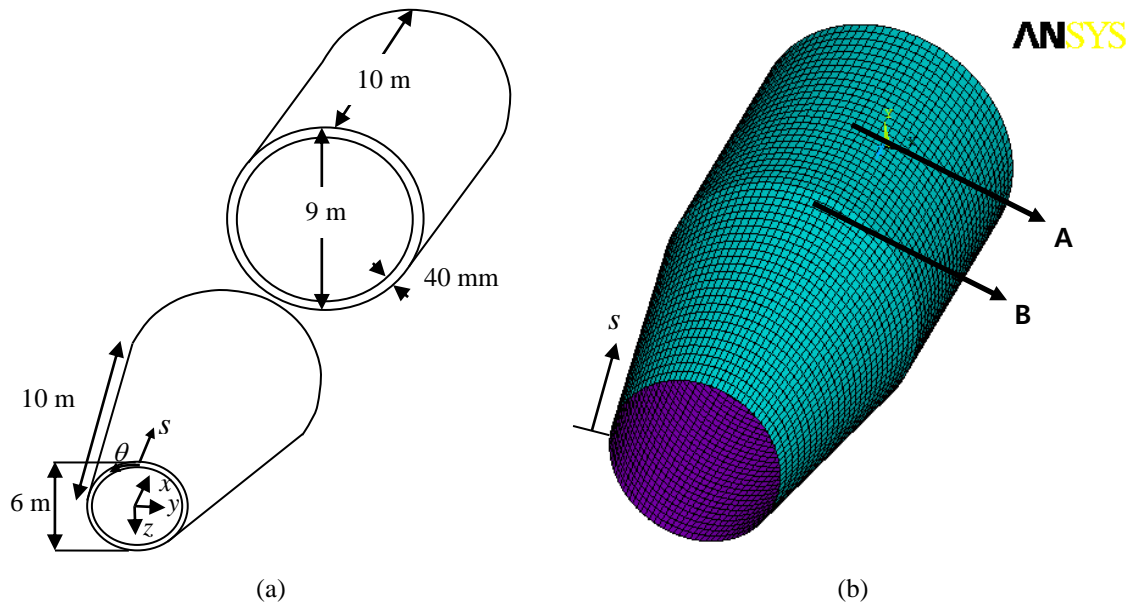The numerical simulation is carried out using finite element package ANSYS 13.0. von-Mises

Fig. 1 (a) Geometry and dimensions of Joined conical cylindrical shell. (b) Finite Element Model

yield criterion and associated flow rule are used together with the Chaboche's kinematic hardening rule in the simulations. An assumption of cyclically stabilized material has been taken. The dimensions of the geometry considered are shown in Fig. 1(a). Eight noded element with six nodal degrees of freedom (SHELL 281) is used for the study. Based on the convergence study, conical-cylindrical shell is discretized with 50 elements along meridional direction and 70 elements along circumferential direction. The finite element discretization of the joined conical cylindrical shell is shown in Fig. 1(b). Two locations have been marked in Fig. 1(b) for presenting the response to cyclic loadings. 'A' denotes the location in cylindrical portion (s=14.8 m) and 'B' denotes the location near the joint (s=9.2 m).

Ratchetting characteristics are investigated for a set of uniaxial and multiaxial loadings. In uniaxial case, asymmetric stress controlled cycling is done. Multiaxial behaviour is demonstrated by applying various combinations of cyclic axial, torsional, internal pressure and bending loading of the thin walled conical-cylindrical shell. It is apt to make a mention here that the elastic or elasto-plastic asymmetric buckling of conical-cylindrical shell under axial stress/strain controlled/torsional/bending loadings is not considered in the present study.

3.1 FE Model validation

The Chaboche model constants for AISI 1026 Carbon Steel are given in Table 1 (Bari and Hassan 2000). The validation of the present approach is carried out considering ratcheting under uniaxial and multiaxial loading of a tubular section of 25.4 mm outside diameter and 1.27 mm thickness. For uniaxial case, one end of the cylindrical shell is clamped and the other end is stress cycled axially. The results for uniaxial simulations are depicted in Fig. 2(a). For multiaxial case, one end of the cylindrical shell is clamped and the other end is axially strain cycled with constant internal pressure on the shell. The results for multiaxial simulations are shown in Fig. 2(b).

Table 1 Material properties of AISI carbon steel (Bari and Hassan 2000)

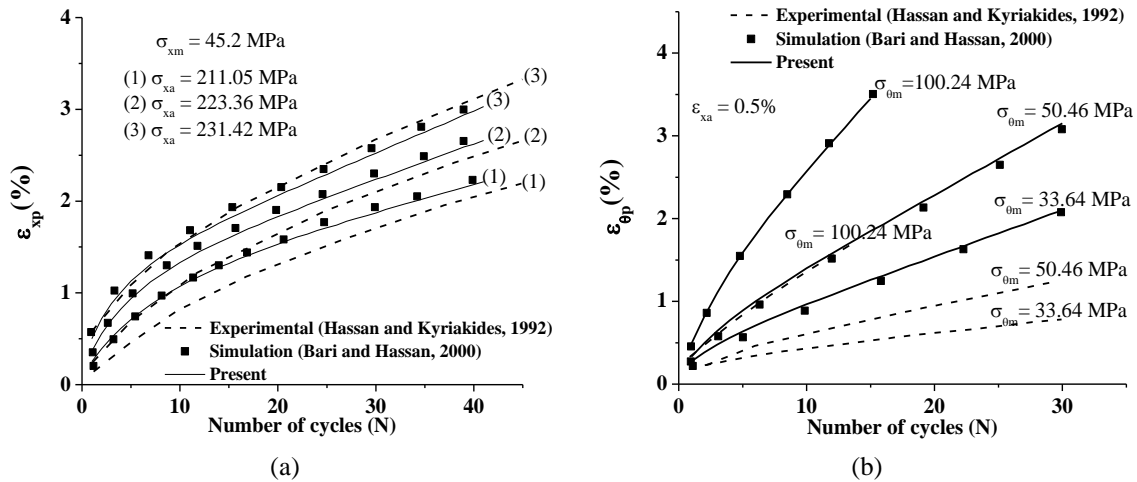| E	σ_y	C_1	C_2	C_3	γ_1	γ_2	γ_3
183 GPa	130 MPa	417.2 GPa	89.4 GPa	3.16 GPa	20000	800	9

Fig. 2 Comparison of simulation and experimental results: (a) axial plastic strain at positive stress peaks of uniaxial cycles, (b) circumferential plastic strain peaks of axial strain cycles with constant pressure
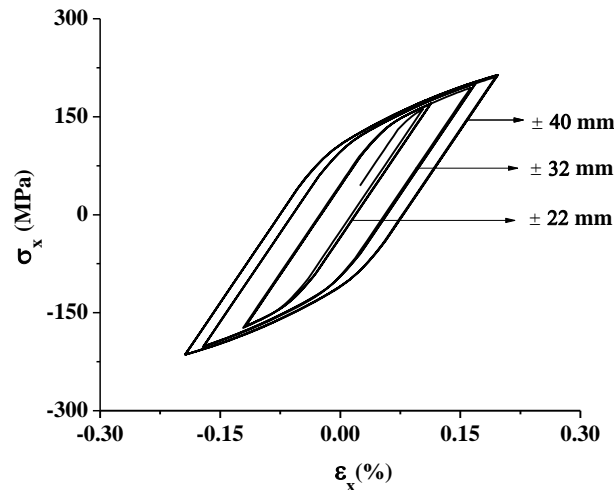

Fig. 3 Stress-strain curves at point 'A' under strain symmetric cycling for different displacement amplitudes

The present results are in good agreement with the simulations (Bari and Hassan 2000) and they follow the experimental trend (Hassan and Kyriakides 1992, Hassan *et al.* 1992) of increase in rate of ratcheting with number of cycles. The difference between simulation and experimental results may be attributed to the inaccuracy in representing the transition region of the stress-strain hysteresis loop from high modulus to low modulus in Chaboche model.
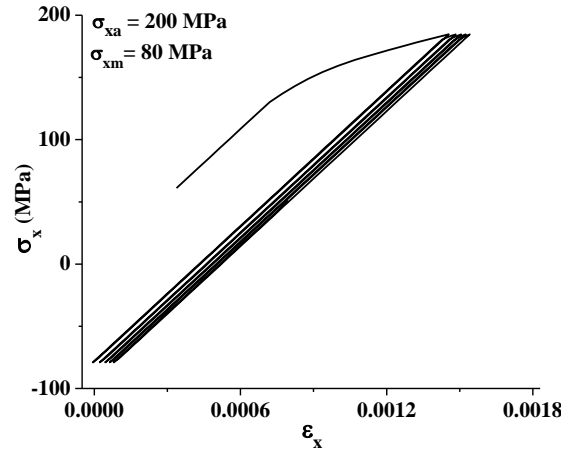
Fig. 4 Stress-strain response at point 'A' under asymmetrical cyclic stress loading
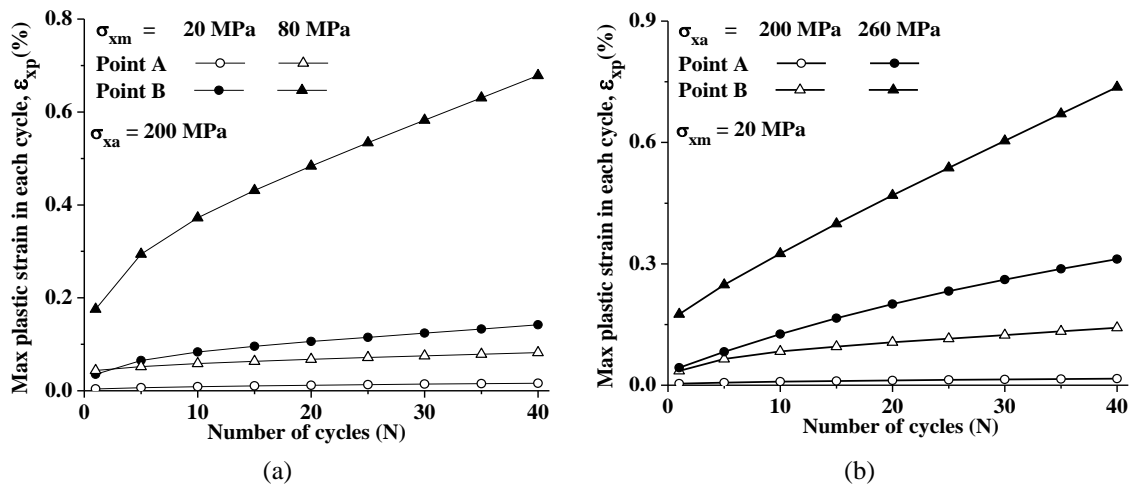

| | |
| (a) | (b) |

Fig. 5 Maximum axial plastic strain as function of the number of cycles in uniaxial ratcheting at points 'A' and 'B': (a) constant stress amplitude (b) constant mean stress

3.2 Strain cyclic begaviour of joined shell

Uniaxial symmetrical strain controlled cyclic simulations are done with variable imposed axial displacement amplitudes as: (1) ±22 mm, (2) ±32 mm, (3) ±40 mm for four loading cycles each. The cylindrical end is clamped and the conical end is axially strain cycled. Fig. 3 shows the simulation results at point 'A' for three displacement amplitudes. The responded stress amplitude σ_x increases with the increase in displacement amplitude. The stress amplitude σ_x becomes immediately saturated when the cyclic strain amplitude is stepped up.

3.3 Ratcheting behaviour of joined shell: uniaxial ratcheting

The analysis is carried out under asymmetrical stress-controlled cycling with positive mean

stress. The cylindrical end is clamped and the conical end is axially stress cycled. Axial stress strain response at point 'A' is depicted in Fig. 4. The induced hysteresis loop never closes, and as a result the plastic strain gradually increases in the direction of the mean stress. The incremental plastic strains in each loading cycle are smaller making the successive hysteresis curves quite close to one another.

To investigate the effect of mean stress and stress amplitude, two sets of simulations are conducted. In the first set, the stress amplitude is kept constant and the mean stress is varied. In the second set, the mean stress is kept constant and the stress amplitude is varied. In Fig. 5, the maximum axial strain in each cycle is plotted as a function of the number of cycles at points 'A' and 'B'. It is clear from Fig. 5 that the two stress cycle variables affect the rate of ratchetting in both set of results presented. Increase in either of these leads to a faster rate of strain accumulation. It is observed that the rate of ratchetting is faster in the first few cycles. As the material hardens, the rate decreases to a constant value.

The accumulated axial plastic strain at the end of 40 cycles is plotted with mean stress and stress amplitude for point 'A' (cylinder) and 'B' (joint) in Fig. 6. The axial plastic strains at the joint are quite large in comparison to the plastic strains in the cylindrical part. It can be observed that as the mean stress or stress amplitude is increased, the accumulated axial plastic strain increases. Fig. 7 shows the variation of axial plastic strain in the meridional direction at the end of 40 loading cycles. The axial plastic strain is maximum at the smaller end of the cone, decreases almost linearly towards the joint and is almost constant over the cylindrical portion. This is attributed to the decrease in the axial stress with the increase in the radius of the conical shell under axial loading. Further, there is a sharp variation of axial plastic strain near the joint due to local bending effects.

Fig. 8 shows the maximum   strain in each cycle plotted as a function of the number of cycles at points 'A' and 'B' for a lower stress amplitude (180 MPa). It can be observed from the figure that yield stress is surpassed and plastic strains develop in the first cycle, there is no cyclic increase of plastic strain in the subsequent cycles at point 'A'. This phenomenon is known as elastic
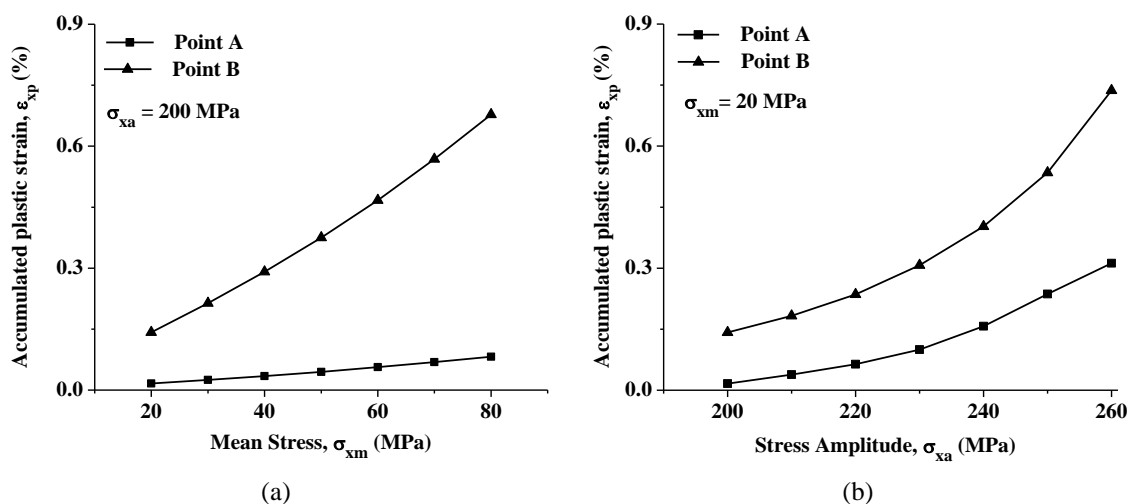

Fig. 6 Maximum axial plastic strain after 40 cycles of uniaxial loading: (a) constant stress amplitude (b) constant mean stress
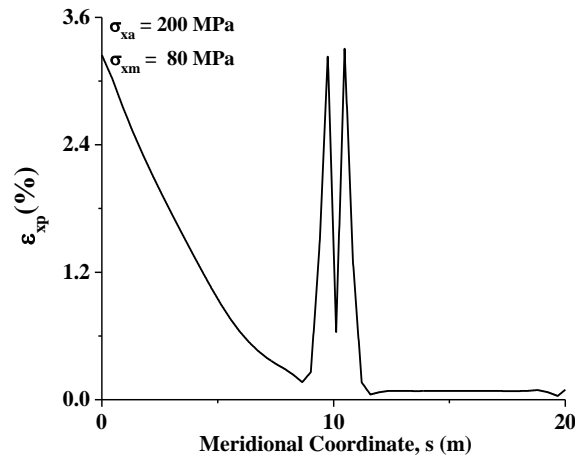
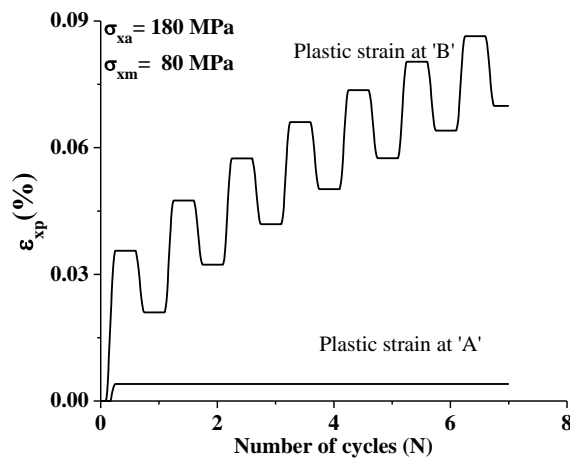Fig. 7 Axial plastic strain variation along the meridional direction (θ=0.0)

Fig. 8 Elastic shakedown at point 'A' and ratcheting at point 'B'

shakedown. However, increasing plastic strains are found to develop near the joint at point 'B'. At point 'A', ratcheting occurs only when stress amplitude is greater than or equal to 200 MPa.

3.4 Ratcheting behaviour of joined shell: multiaxial ratcheting

Ratchetting behaviour of joined conical cylindrical shell under multiaxial asymmetrical stress-controlled cycling is studied for various loading cases.

3.4.1 Internal pressure cycling

Both the cylindrical and the conical ends are clamped and the inner surface is subjected to cyclic pressure. This leads to a progressive increase in the diameter of the shell (circumferential strain ratcheting). The plot of circumferential stress vs. circumferential strain at point 'A' in Fig. 9 depicts ratcheting in circumferential direction.
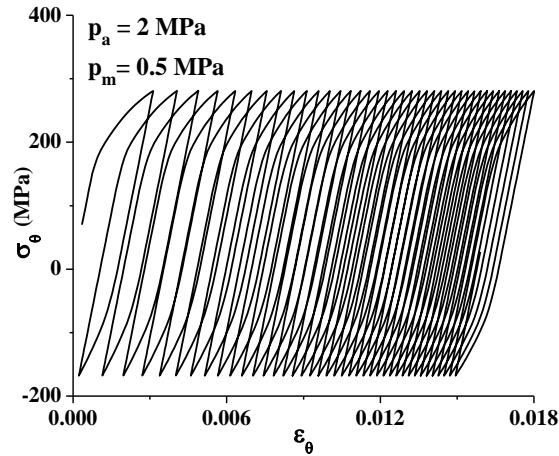
Fig. 9 σ_θ versus ε_θ plot showing ratcheting in circumferential direction at point 'A'
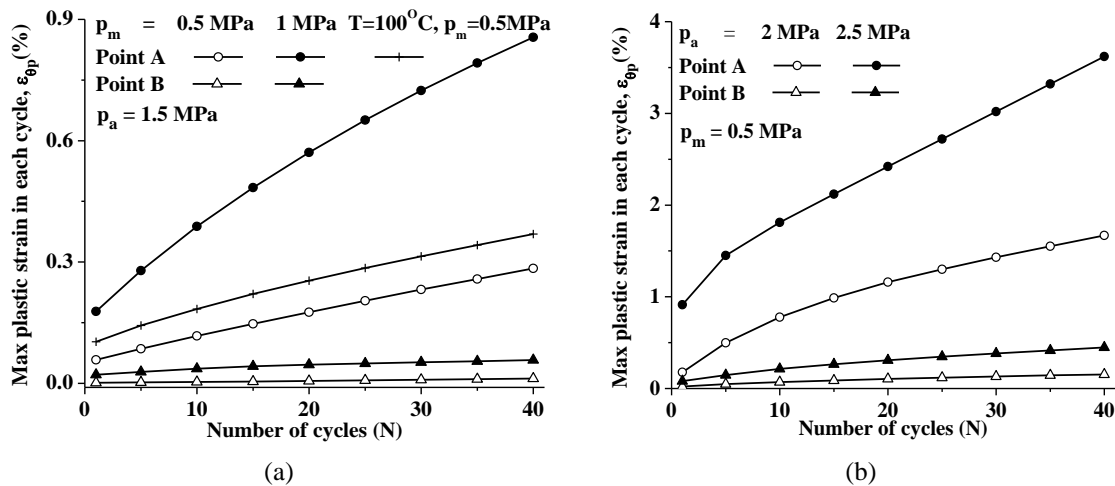
Fig. 10 Maximum circumferential plastic strain in each cycle as a function of the number of cycles at points 'A' and 'B' in asymmetrical internal pressure cycling: (a) constant pressure amplitude, (b) constant mean pressure

To investigate the effect of mean stress and stress amplitude, two sets of simulations are conducted in which the values of mean and amplitude of cyclic pressure are varied. The maximum circumferential strains at points 'A' and 'B' in each cycle as a function of the number of cycles are depicted in Fig. 10. The results in Fig. 10 demonstrate that an increase in mean pressure or pressure amplitude increases the rate of ratchetting similar to axial loading. Fig. 10(a) additionally illustrates that ratcheting strains at 100°C at point 'A' are greater than at room temperature.

The accumulated circumferential plastic strain after 40 cycles is plotted with mean pressure and pressure amplitude for point 'A' (cylinder) and 'B' (joint) in Fig. 11. The plastic strains at the joint are significantly greater in comparison to the plastic strains in the cylindrical section. As the value of mean pressure and pressure amplitude is increased, the accumulated circumferential plastic strain increases. Fig. 12 shows the variation of circumferential plastic strain in the meridional
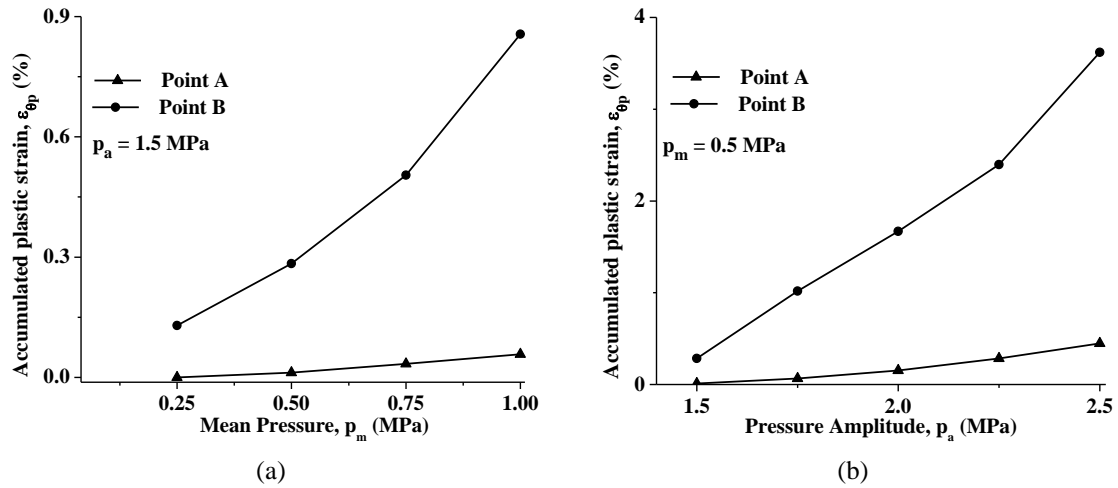
Fig. 11 Accumulated circumferential plastic strains at points 'A' and 'B' after 40 cycles versus pressure in asymmetrical internal pressure cycling: (a) constant pressure amplitude (b) constant mean pressure
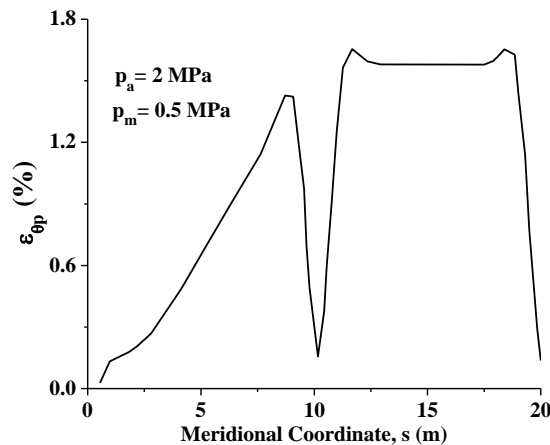

Fig. 12 Circumferential plastic strain variation along the meridional direction (θ=0.0)

direction at the end of 40 loading cycles. The plastic strain is minimum at the smaller end of the cone and increases almost linearly towards the joint. Maximum plastic strain is developed and is almost constant over the cylindrical portion. The observed behavior is different from that of axial loading case and is attributed to the increase in the hoop stress with the increase in the radius of the conical shell under internal pressure. There is a sharp variation of circumferential plastic strain near the joint due to local bending effects.

In order to discuss the ratcheting behaviour under other non proportional multiaxial stress-controlled cycling, study is carried out for constant pressure with axial strain cycling and the result is shown in Fig. 13. It is observed from Fig. 13 that ratcheting at point 'A' occurs in both axial and circumferential directions in comparison to the previous case where it was just in the circumferential direction. But the circumferential plastic strain is greater compared to the axial plastic strain.
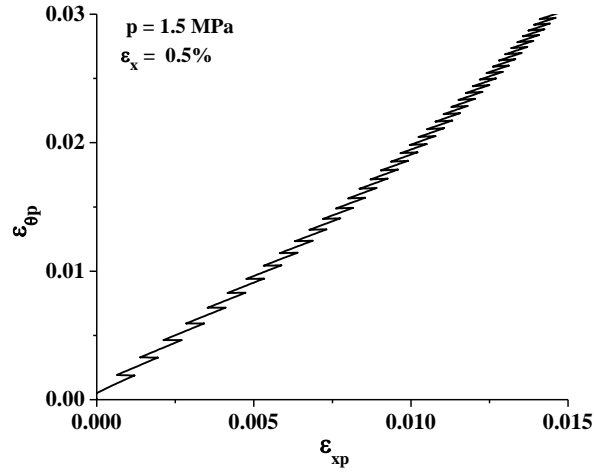
Fig. 13 Circumferential plastic strain versus axial plastic strain at point 'A' under constant internal pressure and axial strain cycling
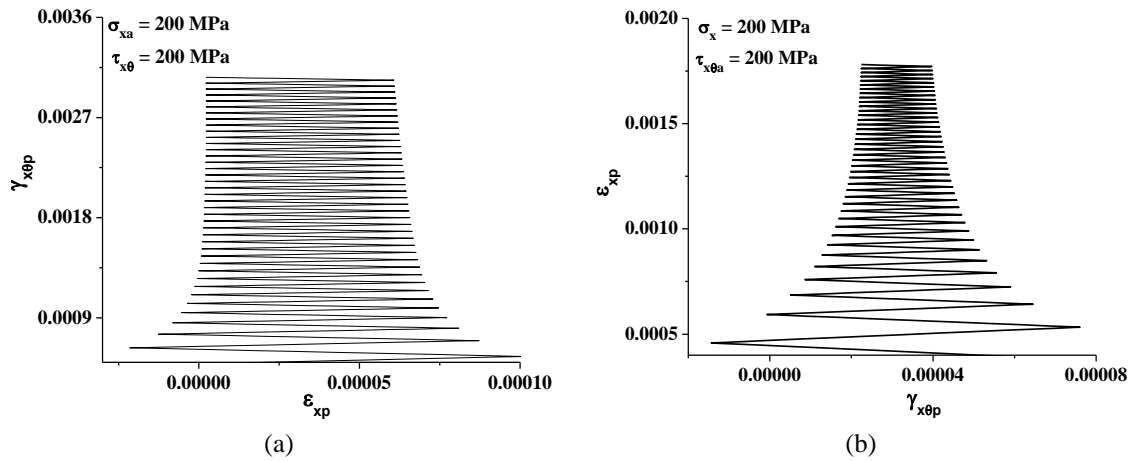
Fig. 14 Torsional plastic strain versus axial plastic strain curves at point 'A': (a) under constant torsional stress with cyclic axial stress, (b) constant axial stress with cyclic torsional stress

3.4.2 Torsional cycling

Two different loading conditions i.e., axial stress symmetric cycling in the presence of constant torsional stress and torsional stress symmetric cycling with constant axial stress are applied on the conical end with the cylindrical end being clamped. The simulation results for torsional strain versus axial strain at point 'A' are shown in Fig. 14. It can be inferred from Figs. 13 and 14 that under nonproportional multiaxial stress-controlled cycling, ratcheting greatly depends on the loading path and mainly appears in the direction of non zero mean stress component.

3.4.3 Cyclic bending

Cyclic bending stress is applied through bending moment about y axis on the conical end with the cylindrical end being clamped. Fig. 15 shows the plot of maximum circumferential and axial
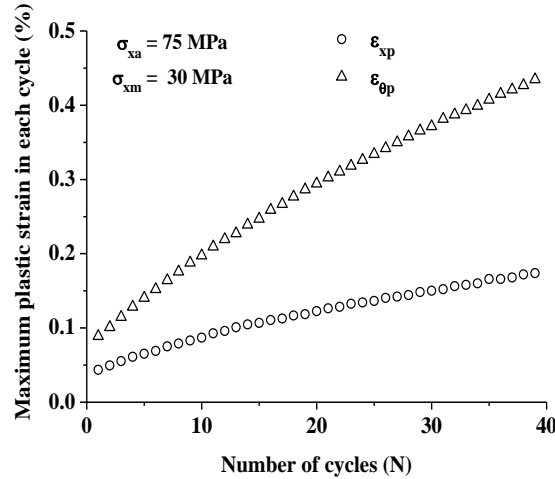
Fig. 15 Variation of axial and circumferential plastic strains at point 'A' with the number of cycles (N) under asymmetrical cyclic bending of joined conical cylindrical shell

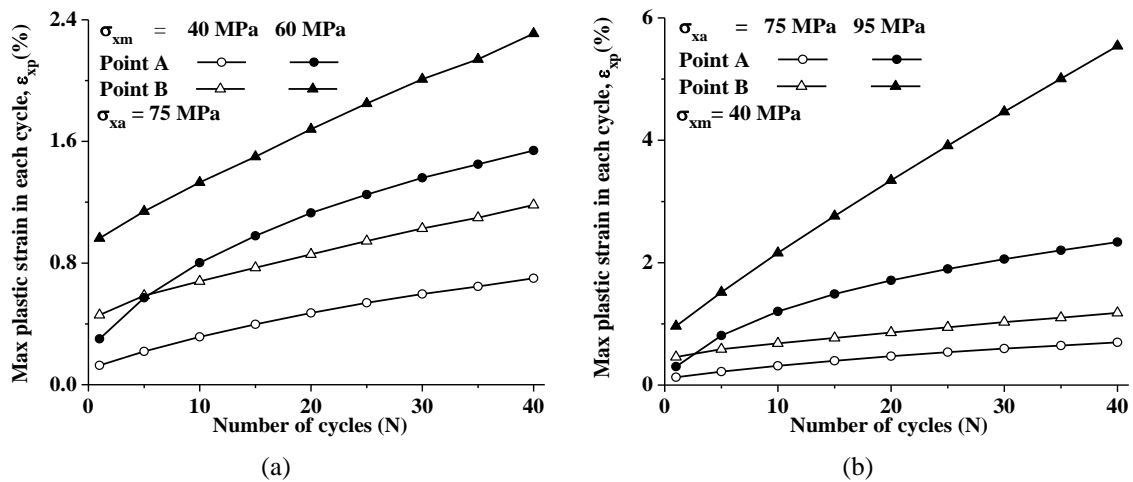(a)   (b)

Fig. 16 Maximum ratcheting strain as a function of the number of cycles in asymmetrical cyclic bending: (a) constant stress amplitude, (b) constant mean stress

plastic strains at point 'A' in each cycle versus the number of cycles. It can be seen from the figure that the axial ratcheting is greater than the circumferential ratcheting.

In Fig. 16, keeping mean stress constant with variable stress amplitude and vice-versa, the maximum axial plastic strain in each cycle is plotted as a function of the number of cycles at points 'A' and 'B'. In Fig. 17, the accumulated axial plastic strain after 40 cycles is plotted with increasing mean stress and stress amplitude for points 'A' (cylinder) and 'B' (joint).

Qualitatively, the results presented in Figs. 16 and 17 are similar to the case of uniaxial ratcheting. Fig. 18 shows the variation of axial plastic strain in the meridional direction. The axial plastic strain is maximum at the smaller end of the cone and shows the nonlinear decreasing trend towards the joint. The plastic strain increases slightly from joint to cylindrical end. The axial
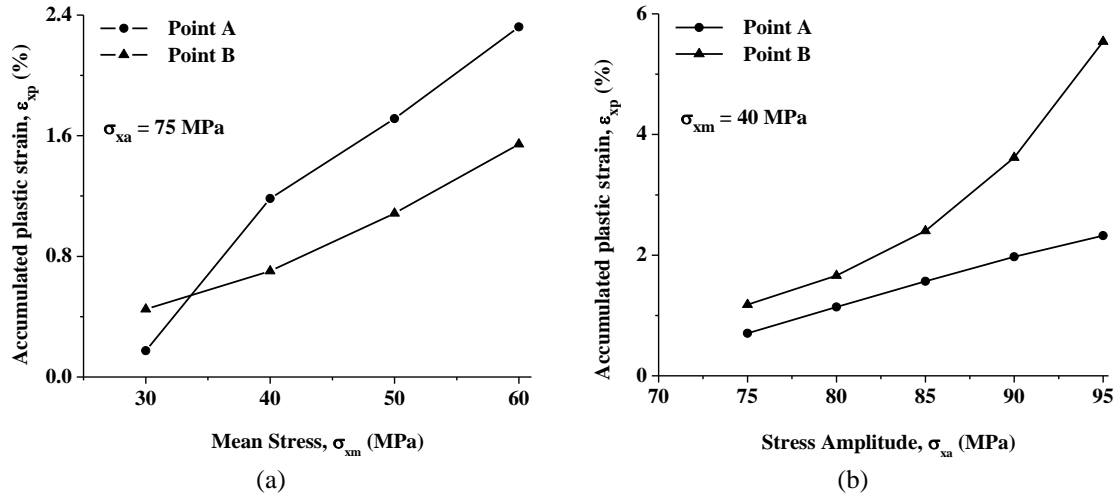
Fig. 17 Accumulated axial plastic strain at points 'A' and 'B' after 40 cycles of asymmetrical cyclic bending: (a) constant stress amplitude, (b) constant mean stress
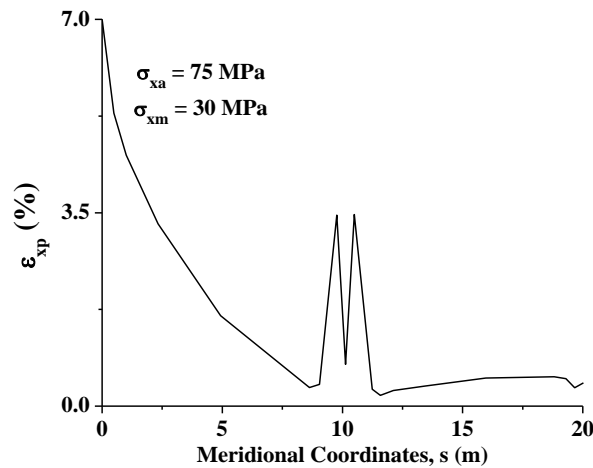

Fig. 18 Variation of axial plastic strain along the meridional direction (θ=0)

plastic strain variation along the circumference of the joint is plotted in Fig. 19. It is observed that the axial plastic strain is maximum but of opposite sign at the two opposite extreme positions of the joint. The plastic strains are close to zero at the middle portion of the joint.

3.5 Dynamic effects on ratcheting behaviour

In order to investigate the effect of inertia on ratcheting, uniaxial ratcheting simulations are carried out in ANSYS 13.0 for different loading frequencies through nonlinear transient dynamic analysis. The range of forcing frequency is decided based on the linear elastic modal analysis. The natural frequency corresponding to the first axial vibration mode of elastic vibration of the joined shell is found to be 62.34 Hz. The transient response analysis is carried out for forcing frequencies
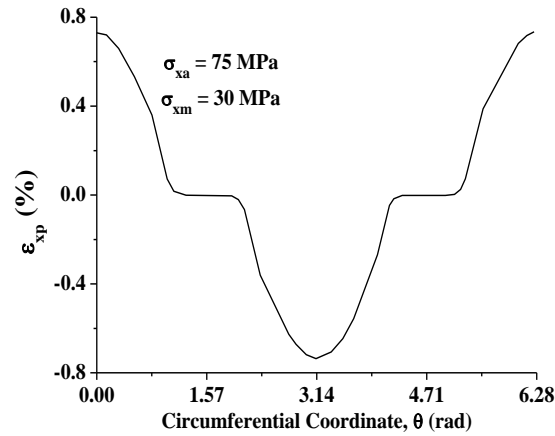
Fig. 19 Variation of axial plastic strain along the circumferential direction at point B (*s*=9.2 m)
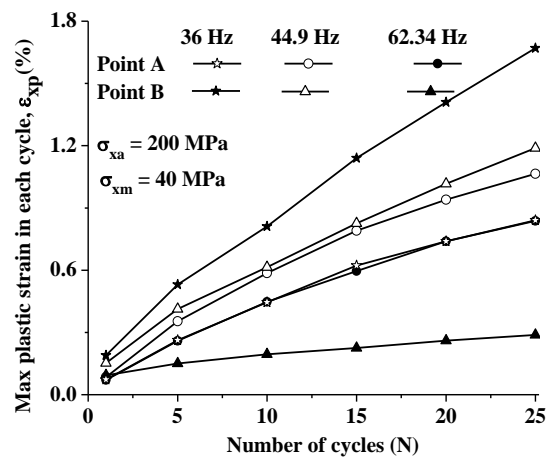

Fig. 20 Maximum axial plastic strain as a function of the number of cycles (N) in uniaxial ratcheting at different loading frequencies
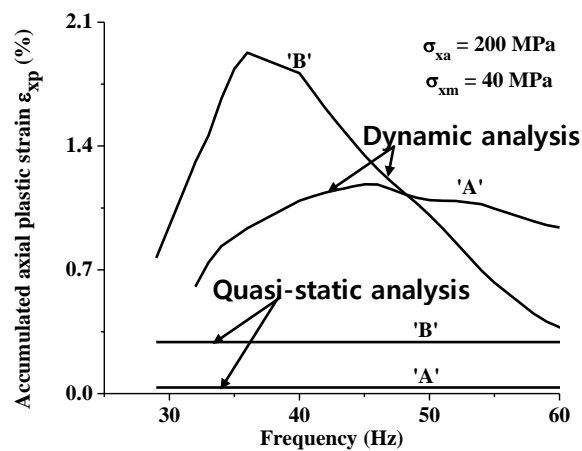

Fig. 21 Accumulated axial plastic strain at 'A' and 'B' after 25 cycles as a function of forcing frequency

in the neighborhood of the first axial mode frequency considering elasto-plastic behaviour. The typical plastic strain history at points 'A' and 'B' are shown in Fig. 20 for 36 Hz, 44.9 Hz and 62.34 Hz forcing frequency. Fig. 21 shows the axial plastic strain at point 'A' after 25 cycles versus forcing frequency. It can be seen from Fig. 21 that the forcing frequency (44.9 Hz) corresponding to peak axial ratcheting strain amplitude is significantly smaller than the natural frequency of first axial elastic vibration mode. This is due to the decrease in effective stiffness in the dynamic elasto-plastic deformation resulting in decrease in resonant frequency. It can also be seen from Fig. 21 that the axial ratcheting strains predicted from dynamic elasto-plastic analysis are significantly greater depending upon the forcing frequency compared to those predicted from quasi-static analysis.

5. Conclusions

Uniaxial and multiaxial ratcheting under different loading conditions is studied using Chaboche model in FE software ANSYS 13.0. It is found that in strain cyclic behaviour, the rate of cyclic hardening increases with the increase in strain amplitude. The ratcheting strain increases with the increase in mean stress and stress amplitude of uniaxial loading. Plastic strain developed near the shell joint is greater than on the cylindrical part in case of uniaxial ratcheting. In case of multiaxial ratcheting (internal pressure cycling), strain developed near the joint is less as compared to cylindrical part. In multiaxial ratcheting (torsional cycling), ratcheting occurs in the direction of mean stress. At higher temperatures, the rate of ratcheting increases. It is concluded from the dynamic analysis that the forcing frequency corresponding to peak ratcheting strain amplitude is significantly smaller than the frequency of first axial elastic vibration mode. The strains predicted from quasi static analysis are significantly smaller as compared to the peak strains from dynamic analysis.

References

Badnava, H., Farhoudi, H.R., Nejad, K.F. and Pezeshki, S.M. (2012), "Ratcheting behavior of cylindrical pipes based on the Chaboche kinematic hardening rule", *J. Mech. Sci. Tech.*, **26**(10), 3073-3079.

Bari, S. and Hassan, T. (2000), "Anatomy of coupled constitutive models for ratcheting simulation", *Int. J. Plast.*, **16**(3), 381-409.

Benallal, A., Le Gallo, P. and Marquis, D. (1989), "An experimental investigation of cyclic hardening of 316 stainless steel and of 2024 aluminium alloy under multiaxial loadings", *Nucl. Eng. Des.*, **114**(3), 345-353.

Benham, P. (1965), "Some observations of cyclic strain-induced creep in mild steel at room temperature", *Int. J. Mech. Sci.*, **7**(2), 81-86.

Besseling, J. (1959), "A Theory of elastic, plastic and creep deformations of an initially isotropic material showing anisotropic strain-hardening, creep recovery, and secondary creep", *Int. J. Appl. Mech.*, **25**, 529-536

Chaboche, J.L. (1986), "Time-independent constitutive theories for cyclic plasticity", *Int. J. Plast.*, **2**(2), 149-188.

Chaboche, J.L. (1991), "On some modifications of kinematic hardening to improve the description of ratchetting effects", *Int. J. Plast.*, **7**(7), 661-678.

Chen, X., Chen, X., Yu, D. and Gao, B. (2013), "Recent progresses in experimental investigation and finite element analysis of ratcheting in pressurized piping", *Int. J. Press. Vess. Pip.*, **101**, 113-142.

Corona, E., Hassan, T. and Kyriakides, S. (1996), "On the performance of kinematic hardening rules in predicting a class of biaxial ratcheting histories", *Int. J. Plast.*, **12**(1), 117-145.

Dafalias, Y. and Popov, E. (1976), "Plastic internal variables formalism of cyclic plasticity", *J. Appl. Mech.*, **43**(4), 645-651.

Delobelle, P., Robinet, P. and Bocher, L. (1995), "Experimental study and phenomenological modelization of ratchet under uniaxial and biaxial loading on an austenitic stainless steel", *Int. J. Plast.*, **11**(4), 295-330.

Dong, J., Wang, S. and Lu, X. (2006), "Simulations of the hysteretic behavior of thin-wall cold-formed steel members under cyclic uniaxial loading", *Struct. Eng. Mech.*, **24**(3), 323-347.

Frederick, C.O. and Armstrong, P. (1966), "A mathematical representation of the multiaxial Bauschinger effect", CEGB Report No. RD/B/N 731.

Hassan, T., Corona, E. and Kyriakides, S. (1992), "Ratcheting in cyclic plasticity, part II: multiaxial behavior", *Int. J. Plast.*, **8**(2), 117-146.

Hassan, T. and Kyriakides, S. (1992), "Ratcheting in cyclic plasticity, part I: uniaxial behavior", *Int. J. Plast.*, **8**(1), 91-116.

Hassan, T. and Kyriakides, S. (1994a), "Ratcheting of cyclically hardening and softening materials, part I: uniaxial behavior", *Int. J. Plast.*, **10**(2), 149-184.

Hassan, T. and Kyriakides, S. (1994b), "Ratcheting of cyclically hardening and softening materials, part II: multiaxial behavior", *Int. J. Plast.*, **10**(2), 185-212.

Jiang, Y. and Kurath, P. (1996), "Characteristics of the Armstrong-Frederick type plasticity models", *Int. J. Plast.*, **12**(3), 387-415.

Jiang, Y. and Sehitoglu, H. (1994), "Multiaxial cyclic ratchetting under multiple step loading", *Int. J. Plast.*, **10**(8), 849-870.

Kang, G. (2008), "Ratchetting: recent progresses in phenomenon observation, constitutive modeling and application", *Int. J. Fatig.*, **30**(8), 1448-1472.

Kang, G., Gao, Q., Cai, L. and Sun, Y. (2002), "Experimental study on uniaxial and nonproportionally multiaxial ratcheting of SS304 stainless steel at room and high temperatures", *Nucl. Eng. Des.*, **216**(1), 13-26.

Mahmoudi, A.H., Badnava, H. and Pezeshki-Najafabadi, S.M. (2011a), "An application of Chaboche model to predict uniaxial and multiaxial ratcheting", *Procedia Eng.*, **10**(0), 1924-1929.

Mahmoudi, A.H., Pezeshki-Najafabadi, S.M. and Badnava, H. (2011b), "Parameter determination of Chaboche kinematic hardening model using a multi objective genetic algorithm", *Comput. Mater. Sci.*, **50**(3), 1114-1122.

Mroz, Z. (1967), "On the description of anisotropic work hardening", *J. Mech. Phys. Solid.*, **15**(3), 163-175.

Ohno, N. and Wang, J.D. (1993a), "Kinematic hardening rules with critical state of dynamic recovery, part I: formulation and basic features for ratchetting behavior", *Int. J. Plast.*, **9**(3), 375-390.

Ohno, N. and Wang, J.D. (1993b), "Kinematic hardening rules with critical state of dynamic recovery, Part II: application to experiments of ratchetting behavior", *Int. J. Plast.*, **9**(3), 391-403.

Rahman, S.M. (2006), "Finite element analysis and related numerical schemes for ratcheting simulation", Ph. D. Thesis, North Carolina State University, Raleigh.

Shariati, M., Hatami, H., Torabi, H. and Epakchi, H.R. (2012), "Experimental and numerical investigations on the ratcheting characteristics of cylindrical shell under cyclic axial loading", *Struct. Eng. Mech.*, **44**(6), 753-762.

Shield, R.T. and Ziegler, H. (1958), "On Prager's hardening rule", *J. Appl. Math. Phys.*, **9a**, 260-276.

Zakavi, S.J., Zehsaz, M. and Eslami, M.R. (2010), "The ratchetting behavior of pressurized plain pipework subjected to cyclic bending moment with the combined hardening model", *Nucl. Eng. Des.*, **240**(4), 726-737.

CC

Nomenclature

$d\varepsilon^p_{eq}$	equivalent incremental plastic strain
C	material constant
N	Number of loading cycles
p_a	pressure amplitude
p_m	mean pressure
$\boldsymbol{\alpha}$	backstress tensor
$d\boldsymbol{\alpha}$	incremental backstress tensor
$\boldsymbol{\alpha}_k$	decomposed backstress tensor
γ	material constant
γ_p	torsional plastic strain
$d\boldsymbol{\varepsilon}^p$	plastic strain increment tensor
ε_x	total axial strain
ε_{xp}	axial plastic strain
ε_θ	total circumferential strain
$\varepsilon_{\theta p}$	circumferential plastic strain
σ_{xa}	axial stress amplitude
σ_{xm}	axial mean stress
σ_θ	circumferential stress
$\sigma_{\theta a}$	circumferential stress amplitude
$\sigma_{\theta m}$	mean circumferential stress
$\tau_{x\theta}$	torsional stress
$\tau_{x\theta a}$	torsional stress amplitude
$\gamma_{x\theta p}$	torsional plastic strain